

Accepted manuscript

As a service to our authors and readers, we are putting peer-reviewed accepted manuscripts (AM) online, in the Ahead of Print section of each journal web page, shortly after acceptance.

Disclaimer

The AM is yet to be copyedited and formatted in journal house style but can still be read and referenced by quoting its unique reference number, the digital object identifier (DOI). Once the AM has been typeset, an ‘uncorrected proof’ PDF will replace the ‘accepted manuscript’ PDF. These formatted articles may still be corrected by the authors. During the Production process, errors may be discovered which could affect the content, and all legal disclaimers that apply to the journal relate to these versions also.

Version of record

The final edited article will be published in PDF and HTML and will contain all author corrections and is considered the version of record. Authors wishing to reference an article published Ahead of Print should quote its DOI. When an issue becomes available, queuing Ahead of Print articles will move to that issue’s Table of Contents. When the article is published in a journal issue, the full reference should be cited in addition to the DOI.

Submitted: 07 April 2016

Published online in ‘accepted manuscript’ format: 01 November 2017

Manuscript title: Experimental investigation of drainage during earthquake-induced liquefaction

Authors: O. Adamidis* and S. P. G. Madabhushi[†]

Affiliations: *IGT, HIL, Stefano-Franscini-Platz 5, ETHZ, 8093 Zrich, Switzerland;

[†]Schofield Centre, University of Cambridge, CB3 0EL, UK

ABSTRACT

Earthquake-induced liquefaction is typically viewed as an undrained phenomenon with undrained element tests forming the core of knowledge built around it. However, there is evidence to suggest that partial drainage could be taking place during an earthquake. In this paper two dynamic centrifuge tests are presented, in which drainage was restricted for a part of the soil by enclosing it within a chamber, in order to assess its importance. The hypothesis of undrained behaviour was found to be inappropriate for liquefied sand, even within the timescale of an earthquake. Fluid flow during the seismic motion was inevitable. Its effect on pore pressures and shear stress - shear strain response was controlled by the proximity of the boundaries.

KEYWORDS: liquefaction; drainage; fluid flow

INTRODUCTION

Undrained element tests form the basis of our understanding of earthquake-induced liquefaction. The principal hypothesis behind these tests is that during earthquake loading, drainage through liquefied sand is slow enough to be neglected. An example of a thorough framework for liquefaction, as understood through undrained tests, is given by Ishihara (1993). This and other similar frameworks use undrained tests to estimate both the onset and the consequences of liquefaction.

Such frameworks are dependent on the validity of the undrained hypothesis, which has come under scrutiny by researchers working on a general formulation for liquefaction. Goren et al. (2010) describe two mechanisms that contribute to liquefaction. The first is pore volume compaction and the second is fluid flow. They point out that boundary conditions prescribe which mechanism is of importance and they state that in the field, during liquefaction of sand, both mechanisms are expected to operate together. Undrained tabletop experiments can only capture the first of the two mechanisms. Lakeland et al. (2014) also criticise undrained element experiments for their inability to incorporate flow, stating that ‘under the ground, water flow is extremely important and tabletop experiments, as currently performed, simply cannot model this process’. Instead, they recommend dynamic centrifuge tests.

Efforts to examine the effect of fluid flow using element tests have been made. Boulanger & Truman (1996) performed triaxial tests with water injection to model an element of sand underneath a low permeability layer. They observed that due to fluid inflow the soil dilated until it reached instability. Vaid & Eliadorani (1998) performed triaxial tests under partially drained conditions, allowing water inflow or outflow in a controlled manner. They pointed out that an extremely small volumetric expansion due to water inflow is sufficient to lead a sand sample that would be stable under undrained loading towards instability. Vaid & Eliadorani (2000) also demonstrated that the degree of partial drainage controls the direction of the effective stress increment and the deformation response. Moreover, the shear resistance of sand was shown by Sento et al. (2004) to be very sensitive to volume change due to water inflow. All in all, a soil element’s response in the field should not be expected to be bounded by drained and undrained test results in terms of either stiffness (Vaid & Eliadorani (2000)) or strength (Kamai & Boulanger (2012)).

The above experiments established the shortcomings of typical undrained element tests but did not reveal any information regarding the timescale of drainage, a vital part of the undrained hypothesis. Such information can be gleaned from studies that examine the formation of water films between a layer of liquefiable sand and an overhead layer of lower permeability. Kokusho (2003) observed that such water films form just after the onset of liquefaction. In other words, void redistribution and fluid migration can happen during the earthquake and are therefore much faster than assumed by the undrained hypothesis. This observation is in line with the estimations of the timescale of pressure diffusion stemming from theoretical formulations, such as those by Goren et al. (2010) or Lakeland et al. (2014). Research implies that fluid migration could take place during an earthquake and lead sand elements closer to instability. As a result, there is a need to reassess the validity of the undrained hypothesis, which remains a widely used assumption. Indeed, the undrained hypothesis is still routinely used in practice to perform seismic response analysis of sites which contain liquefiable soil. In this paper, experimental results from two dynamic centrifuge tests are presented, providing evidence against the use of the undrained hypothesis for liquefaction-related problems.

EXPERIMENTAL METHODS

Two geotechnical centrifuge experiments were performed, named OA2 and OA3. Centrifuge tests were selected as the only type of experiment that allows realistic conclusions to be drawn regarding the significance of drainage during liquefaction in the free-field. A cross section of the models tested is depicted in figure 1. On one side of each model, a part of the soil was enclosed in a chamber which restricted the inflow and outflow of pore fluid. On the other side, an instrumented soil column captured the behaviour expected at the free-field.

The use of centrifuges in geotechnics is well documented (for instance, see Madabhushi (2014)). A centrifuge allows the use of scaled-down models while preserving the stress-strain behaviour of soils by scaling up the acceleration of gravity. Stress and hydraulic gradients, soil stress-strain response, and fluid flow can be accurately reproduced.

The model container was a laminar box, consisting of 25 horizontal sections, separated by roller bearings. The sections could move relative to one another, reducing boundary effects. A thin latex barrier between the sections and the sand contained the pore fluid. More information on this laminar box can be found in Brennan et al. (2006).

The sand layers were prepared by air pluviation of Hostun sand, using the automatic sand pourer described in Madabhushi et al. (2006). Some important properties of this sand are included in table 1. Hostun sand has been extensively investigated in element tests (e.g. Azeiteiro et al., 2017; Escibano & Nash, 2015). The targeted relative density was 40%. The chamber for each test was placed when the height of the sand reached the right level. Sand pouring continued with sand being poured inside and outside of the chamber at the same time. Once the chamber was full, it was sealed before the sand pouring continued.

The instrumentation used consisted of miniature piezoelectric accelerometers, pore pressure transducers (PPTs), and linear variable displacement transducers (LVDTs). The layout and the labels of the instruments used can be found in figure 1. Data from displacement transducer L3 were only available for test OA3.

A different type of cylindrical chamber was used for each test. Sketches of the chambers are given in figure 2. The base and the top of the chamber consisted of Perspex disks, 5 mm in thickness and 93 mm in diameter (figure 3a). At the centre of the disks, 90° fittings were placed, to which $\varnothing 6$ mm pipes were connected. Thin cylinders of porous paper were placed between the fittings and the sand inside each chamber. The porous paper allowed fluid to flow through it but prevented sand particles from moving into the pipes.

For test OA2, the periphery of the chamber was made using a latex sheet of 0.3 mm thickness (figure 3b). The latex sheet was sealed to the base using two beads of aquarium silicone. Hostun sand grains were stuck to any surface that would come in contact with the soil (figure 3e,f). During sand pouring, a thin plastic cylinder was used to hold the latex sheet in place. Once the chamber was full, the top cap was placed and the latex was sealed to it, again using two beads of aquarium silicone. After 24 hrs, the silicone was dry, the supporting plastic cylinder was removed, and the sand pouring continued. This chamber could shear along with its surrounding soil and it could also expand laterally.

For test OA3, the goal was to prohibit lateral expansion of the chamber, in a design reminiscent of a simple shear test container. It was important that the chamber remained light so as not to sink during liquefaction. Initially, a latex sheet of 0.3mm thickness was used to form a cylinder. Then, a thin layer of Tylon latex liquid rubber was applied and before it dried, fishing line Maxima Chameleon (18lbs strength, 0.4mm thickness) was wrapped around the chamber, leaving no gaps. Finally, a second coat of liquid rubber was applied. Hostun sand grains were stuck on both sides of this barrier. This procedure was performed for the first 95mm of the chamber's height (figure 2). In order to allow upwards movement of the cap of the chamber without requiring the membrane to stretch, a 15mm tall ring was created for the top of the chamber, within which the cap could move. The ring consisted of a PET cylinder, reinforced with fishing line and slow-setting epoxy resin. A thin bead of aquarium silicone connected it to the rest of the chamber (figure 3d). As in test OA2, once the chamber was full of sand, the latex sheet was sealed to the cap with two beads of aquarium silicone. The latex sheet was folded as shown in figure 2, allowing the top disk to move without stretching the latex. A thin layer of grease between the ring and the latex further facilitated the movement of the cap.

The sand was saturated using a high viscosity aqueous solution of hydroxypropyl methylcellulose, prepared as described in Adamidis & Madabhushi (2015). A viscous solution was used in order to overcome the inconsistency between the scaling laws of dynamic and seepage time in centrifuge modelling (Madabhushi (2014)). The centrifugal acceleration applied was $50g$, so the targeted viscosity of the pore fluid was $50cSt$. However, due to the sensitivity of the hydroxypropyl methylcellulose solution's viscosity to temperature, the actual viscosities during the tests were $42cSt$ and $37cSt$ for OA2 and OA3 respectively. The saturation of the model was performed using the computer controlled system described in Stringer & Madabhushi (2009). A system of pipes was in place for the saturation of the chamber, shown in figure 4. During saturation, both valves of the system were open. Once saturation finished and fluid was seen coming out of the top pipe of the chamber, the vacuum was released. Valves 1 and 2 were then closed and remained this way until the experiments.

The experiments were performed on the Turner Beam Centrifuge, at the Schofield Centre of the University of Cambridge. Before each earthquake, valve 2 was closed. It was opened again after the earthquake was over and the excess pore pressures in the free-field had dissipated. The input motions were sinusoidal, pseudo-harmonic, and were generated using the stored angular momentum (SAM) actuator described in Madabhushi et al. (1998). The targeted duration was $0.4s$ ($20s$ in prototype scale) and the targeted frequency was 50Hz (1Hz in prototype scale). The amplitude increased with each subsequent earthquake. The two first earthquakes will be presented for each test.

RESULTS

The presence of a chamber within the right half of the soil inside the laminar box did not affect the excess pore pressure generation and dissipation process for the free-field soil column, monitored within the left half of the laminar box (figure 1). The time histories of excess pore pressure for the free-field soil column are given in figure 5 and represent a

typical response for a soil column of liquefiable sand. The base of the soil did not reach full liquefaction during the first earthquake, whereas it liquefied fully during the second, stronger motion. The excess pore pressure dissipation process for this column was analysed in Adamidis & Madabhushi (2016), where it was shown that one-dimensional reconsolidation is sufficient to accurately predict the experimentally observed pressures. As a result, any effect from the presence of the chambers was negligible regarding pore pressures within the instrumented soil column at the left half of the model.

Time histories for excess pore pressures are presented in figure 6. Pressures as recorded inside the chamber (PPTs P4 and P6) and at similar depths of the free field (P3 and P5) are depicted. P6 was placed slightly higher than P5 during test OA3. In the same figure, the settlement of the free-field (ff) is shown, as recorded by LVDT L1. Positive displacement corresponds to settlement. Chamber displacement (ch) is also included. For test OA2, this displacement corresponds to the trace of L2. For test OA3, it corresponds to the change in height of the chamber, calculated using L2 and L3. L2 dominated the change in height. Positive displacement signifies a reduction in height for the chamber. Finally, the input acceleration is plotted.

The time axis is split into three parts of different scale. Within each part, time advances linearly between the two end values. Plots are separated at the endpoints of each time window by double lines. The first time window corresponds to the build up of excess pore pressures. The second time window contains rest of the co-seismic response. The third window presents the post-earthquake behaviour.

THEORETICAL IMPLICATIONS OF DRAINAGE

A diffusion equation is commonly used to describe the processes that occur prior to excess pore pressure becoming equal to the level of initial vertical effective stress. These processes most accurately correspond to the first time window of figure 6. For instance, Snieder & Van Den Beukel (2004) derived the following equation:

$$\frac{\partial p}{\partial t} = K_f \left(\nabla \cdot \frac{k}{g \rho_f} \nabla p \right) + K_f \frac{\partial \beta}{\partial t} \quad (1)$$

where p is excess pore pressure, t is time, K_f is the bulk modulus of the pore fluid, k is the hydraulic conductivity, ρ_f is the density of the pore fluid, and β is the grain fraction, equal to the volume of grains over the total volume of an element. If e is the voids ratio, $\beta = 1/(1+e)$. A typical consolidation equation only contains the first term on the right hand side of the above equation, which is related to drainage. However, equation 1 also includes a second term that accounts for pore pressure generation due to compaction. Similar expressions have been proposed by other researchers, such as Wang (2000), Goren et al. (2010) and Lakeland et al. (2014).

Using the first right hand side term of equation 1, Snieder & Van Den Beukel (2004) derived a dimensionless factor for the relative importance of drainage as follows:

$$F = K_f \frac{\left(\nabla \cdot \frac{k}{g \rho_f} \nabla p \right)}{\partial p / \partial t} \quad (2)$$

They considered drainage important if $F > 1$. In the case of a liquefiable layer of thickness L and for a timescale of the liquefaction process T , equation 2 is approximately:

$$F \approx \frac{K_f k T}{g \rho_f L^2} \quad (3)$$

Using this equation, the values corresponding to F were calculated for the free-field and the chambers of the centrifuge tests described above. The results are presented in table 2. The depth of the liquefiable layer was taken as $L = 245 \text{ mm}$ for the free-field column and $L \approx 95 \text{ mm}$ for the chamber, both in model scale. As equation 3 refers to the processes before liquefaction is reached, the timescale T chosen corresponded to the first time window of figure 6, while excess pore pressures were building up. The bulk modulus of the fluid was taken as that of water $K_f = 2.2 \cdot 10^9 \text{ Pa}$ and the hydraulic conductivity as $k = 10^{-3} \text{ m/s}$ (table 1).

As seen from the values of F in table 2, drainage should be considered important in all cases. However, F took values more than six times larger inside the chamber versus at the free-field. Since the timescale for the generation of excess pore pressure was similar inside and outside of the chambers, the differences in F were due to the proximity of the boundaries (term L^2 in equation 3), with drainage becoming more significant as the boundaries approached. While the chambers introduced here prohibited fluid flow out of them, the proximity of the boundaries they introduced made the effect of drainage more significant within them. Drainage within the chambers manifests as void redistribution. In order to attain factors $F < 1$ and consider drainage unimportant for the timescale of the first earthquake applied here, a layer of depth $L > 600 \text{ mm}$ should have been modelled. This depth corresponds to $L > 30 \text{ m}$ in prototype scale; rather large for most cases of earthquake-induced liquefaction.

Lakeland et al. (2014) derived an equation which, if thermal effects are neglected, is in essence similar to equation 1. They performed a non-dimensionalisation of variables using characteristic scales relevant for the liquefaction of soil layers and chose scale constants so that all relevant terms in their equation would have a coefficient equal to unity for typical conditions of soil liquefaction. This allowed them to distinguish the relevant importance of each factor. Following this procedure they derived the following expression for the diffusion timescale Δt :

$$\Delta t = \frac{\phi_0 \mu P_0^2}{g^2 \kappa_0 K_f \rho_f^2} = \frac{\phi_0 \mu \Delta z^2}{\kappa_0 K_f} \quad (4)$$

where P_0 is a reference pressure, ϕ_0 is a reference porosity, μ is the viscosity of the pore fluid, and κ_0 is a reference permeability (in m^2). Δz is a length scale, with $\Delta z = P_0 / (\rho_f g)$. Here, the following values are appropriate: $P_0 = 50 \text{ kPa}$, as this is approximately the level to

which the excess pore pressures examined in figure 6 rise, $\phi_0 = 0.452$ based on the initial relative density of the sand, $\mu \approx 40 \text{ mPa} \cdot \text{s}$, and $\kappa_0 = (k\mu)/(\rho_f g) = 8.15 \cdot 10^{-11} \text{ m}^2$, since the hydraulic conductivity of Hostun sand is $k = 1 \text{ mm/s}$ (table 1). In model scale, where the acceleration of gravity is increased, the resulting length scale is $\Delta z \approx 100 \text{ mm}$, similar to the height of the chambers, and the diffusion timescale is $\Delta t \approx 0.001 \text{ s}$. Clearly, this value is very small, not just compared to the duration of the motion, but also compared to the time of excess pore pressure build up, or even compared to the period of one loading cycle (0.2 s). In other words, fluid flow will very quickly spread localised pressure differences, making an undrained approximation inappropriate for the interpretation of the experimental results.

CO-SEISMIC RESPONSE

The first time window of figure 6 contains the excess pore pressure build up. Excess pore water pressures were generated fast, leading the soil inside the chamber to full liquefaction during all events. The initiation of liquefaction required three to four cycles for the first, smaller earthquake, while only two cycles were necessary for the second, stronger event. The initial rate of excess pore pressure generation was similar inside and outside of the chamber. A significant discrepancy was only observed for the second earthquake of OA2, when a large acceleration half-cycle pushed the sand towards dilative response. In the free-field, where the boundaries were further away, smaller drops in excess pore pressure were observed than within the chamber. Based on the considerations of the previous section, one can attribute this difference to the proximity of the lower boundary of the chamber, where there could be no fluid flow, forcing the gradient of excess pore pressure to zero. The consequent lower level of fluid inflow at the position of the PPTs inside the chamber could have resulted in the more significant drop of excess pore pressure.

In an undrained element test, where boundaries are significantly closer compared to the prototype scale of the presented centrifuge tests, there is practically no spacial variation in excess pore pressure and hence no fluid inflow or outflow. The results of such a test should therefore not be taken as directly representative of reality, where the difference between fluid inflow and outflow can have a significant effect on the evolution of excess pore pressure.

In the following sections the second time window of figure 6 is examined, corresponding to the response after the onset of liquefaction. Initially, the focus is on excess pore pressure traces, followed by displacements.

Excess pore pressures

Full liquefaction was reached at the level of the PPTs included in figure 6, both inside and outside of the chamber. However, at a greater depth, the sand only liquefied during the second, stronger earthquake of each test.

During the first earthquake, excess pore pressures maintained their elevated values, both inside and outside of the chambers, for the duration of the seismic motion. On the contrary, during the second earthquake, excess pore pressures inside the chamber started dropping immediately, even as the earthquake continued. Though the sand was slightly denser during the second motion, the effects of drainage, or of the first right hand side term of equation 1 cannot be expected to differ drastically for the two motions. Instead, the difference observed in excess pore pressure response is likely due to the effect of the second right hand side term, which is related to the deformation of the soil skeleton. This term can be related to shearing, as for instance by Miyamoto et al. (2004). Large levels of shearing result in large levels of excess pore pressure generation and can thus mask the significance of void redistribution that would normally result in the dissipation of excess pore pressure. Here, perhaps counter-

intuitively, larger shearing at the level of the PPTs examined in figure 6 occurred for the first, weaker motion. This was due to the fact that the second, stronger earthquake quickly led the whole layer to liquefaction, softening the sand at the base of the box and limiting shear strains for the rest of the layer, as is discussed in more detail in the following ‘shear stress - shear strain response’ section.

During the second event, the effects of drainage and void redistribution became evident. The time histories of figure 6 point to the formation of a water film below the cap of the chamber. Research on the formation of water films due to liquefaction focuses on liquefiable layers capped with other, low permeability layers. Kokusho (2003) points out that water films can form beneath the layer of lower permeability just after the onset of liquefaction, due to rapid fluid flow. Then, excess pore pressures below the water film dissipate until they reach its level of pressure. This behaviour matches the pressures recorded inside the chamber during the second earthquake. Excess pore pressures dissipated until, after the end of the earthquake, they reached a value of about 35kPa for test OA2 and 28kPa for test OA3. These values corresponded to the pressure of the fluid film and were equal to the initial (pre-earthquake) vertical effective stress at the level of the cap of the chamber. Lower pressure was recorded for test OA3, as that chamber was slightly taller and its cap was closer to the surface (figure 2). The excess pore pressure dissipation process is demonstrated in figure 7, up to the point when excess pore pressures outside of the chamber matched those inside of it, after the end of the earthquake. Figure 7 also presents the isochrones of excess pore pressure dissipation for the first earthquake. However, this process is entirely part of the post-earthquake response and is discussed later.

In the free-field, at the level examined in figure 6, the soil remained liquefied, retaining its elevated excess pore pressures in all cases. Such response is often viewed as undrained. However, the importance of drainage cannot be neglected for a layer of this depth, as previously discussed. If we simplistically consider undrained loading and for the purposes of this argument assume equation 1 to apply, its first right hand side term, related to diffusion, would have to be neglected. Neglecting drainage, the settlement observed at the soil surface has to be attributed to deformation of the soil skeleton. Let's assume that this deformation is the same throughout the layer and has a constant rate which results in surface settlement of about 1mm in about 0.2s (both realistic values based on the traces of figure 6). The resulting

grain fraction change would be $\frac{\partial\beta}{\partial t} \approx 4 \cdot 10^{-3} \text{ s}^{-1}$. Based on equation 1, without accounting for

drainage, such a change would result in excess pore pressures of about 8.8MPa in 0.2s . Clearly, considering the diffusion term as negligible is not an appropriate assumption as it requires unrealistically high fluid pressures to reach the settlement rates observed. In reality, settlement is the result of fluid flow towards the surface of the layer, which takes place both during and after an earthquake. The evolution of excess pore pressures is better viewed as a result of the interplay between continued agitation, which affects the soil skeleton, and fluid flow due to pressure gradients.

Displacements

The displacement response was different for each test. The height of the chamber slightly reduced in OA2, whereas it increased in OA3.

It should be pointed out that rocking of the soil mass occurred during the earthquakes, as can be seen from the traces of L1 and L2 (figure 9). They both oscillated with the input acceleration, albeit not significantly, and when one recorded a peak the other recorded a valley. If a displacement field were to be drawn, its vectors would divert vertically close to the edges of the box, resulting in slightly larger horizontal components towards the centre. Moreover, the cap of the chamber was slightly heavier than sand. The perspex disk, along with the metal fitting and the LVDT rod pictured in figure 2 resulted in an increase of vertical pressure of about $2kPa$ for the soil inside the chamber, compared to soil of the free-field at the same depth. This extra pressure was too small to have any visible effect before the soil liquefied completely.

A possible explanation for the displacement response of the chamber of test OA2 is depicted in figure 8. While the soil was moving towards the chamber, the side of the chamber closer to the centre moved slightly more, due to the rocking of the soil mass. Consequently, the initially circular section BB of figure 8a distorted into an ellipse. This distortion resulted in a reduction of the enclosed area A. It is reminded that according to the isoperimetric inequality, for a given perimeter, it is the circle that contains the maximum area. Since the total volume inside the sealed chamber was practically constant, the aforementioned reduction in area resulted in a temporary increase of the height of the chamber. During the next half cycle, when the soil movement reversed, section BB likely returned to a more circular shape (figure 8b) and the height of the chamber decreased. Due to the weight of the cap, downwards movement was accumulated with each cycle, allowed by the possibility of gradual expansion of the flexible periphery of the chamber.

In OA3, the presence of the fishing line along the periphery of the chamber increased the asymmetrical response. Along a horizontal plane, the periphery of this chamber did not provide additional resistance when pushed into, but did resist when pulled, as only small deformations were required before the fishing line could work in tension. During half-cycles when the soil moved towards the chamber, a horizontal section could get distorted as drawn in figure 8c. Since the perimeter of section BB was constant due to the presence of the fishing line, distortion from the original circular shape resulted in a decrease of the enclosed area A, which forced the chamber to increase in height. Some rotation of the top cap should also be expected from the distorted shape depicted in figure 8c. Indeed, after the end of OA3, when the soil was excavated, residual rotation in this direction was observed (figure 11c). During the half-cycles when the soil moved away from the chamber, deformations as sketched in figure 8d could be expected. The side of the chamber closer to the centre experienced larger horizontal movement, somewhat restoring the chamber's initial shape and causing a temporary lowering of the cap. Since the height of the chamber increased slightly with each cycle, the shape of section BB of figure 8d did not return to its initial circular shape. Instead, it kept on deviating slightly further from a circle with each cycle. The rate of distortion and hence increase in height reduced as effective stresses inside the chamber increased, allowing the sand to better resist movement.

For both tests, peaks of upwards displacement of the cap corresponded to valleys of excess pore pressures in the chamber and vice versa (figure 10). When the cap was moving upwards (figures 8a,c), deformations were reminiscent of strain controlled extension tests and the sand responded with a drop in excess pore pressure, as is also seen at the beginning of undrained extension element tests for Hostun sand (e.g. Doanh et al. (1997)). When the cap moved

downwards (figures 8b,d), deformations were similar to strain-controlled compression tests and the sand responded with an increase in excess pore pressure, as in undrained compression tests for Hostun sand (Doanh et al. (1997)).

Overall, the displacement behaviour of the chambers was controlled by the boundary conditions imposed by their periphery. Transient changes in the shape of the chamber produced oscillations in height within each loading cycle. The expandable periphery of the chamber of OA2 resulted in the gradual decrease of the chamber's height whereas the constant perimeter of the membrane of the chamber in OA3 resulted in the gradual accumulation of upwards movement for the cap.

POST-EARTHQUAKE RESPONSE

The reconsolidation of the free-field was similar for both tests. As no more excess pore pressures were produced due to dynamic shearing, fluid flow led to their gradual dissipation. The reconsolidation of the free-field of these tests can be fully described by a consolidation equation, as long as soil properties are accurately accounted for, as discussed in detail in Adamidis & Madabhushi (2016). An interesting observation related to drainage is that for a certain time after the end of the earthquake and before the arrival of the solidification front, excess pore pressures remained unchanged, as seen for P3 and P5 in figure 6. This response was not undrained as one might hypothesise. Instead, fluid flowed through the sand, as dictated by the settlement of the soil surface. No temporal change in pore pressure occurred because the distribution of excess pore pressures with depth was linear, as imposed by the top boundary condition, and the second order spacial derivative of excess pore pressure was zero, signifying that fluid inflow was the same as fluid outflow for that element.

Inside the chambers, reconsolidation was controlled by the top boundary condition for pressure, in other words by the pressure of a potential fluid film formed below the cap of the chamber. In OA2, the flexible membrane demanded that the pressure of the fluid film was equal to the total horizontal stress outside of the chamber. In OA3, the ring of constant perimeter surrounding the fluid film (figure 2) could develop hoop stresses and withstand differences of pressure along its two sides. Therefore, the boundary condition was defined by the vertical stress imposed by the cap.

After the end of the earthquakes, excess pore pressures inside the chambers dropped to match the boundary condition imposed by a potential fluid film. This is seen in figure 7, where excess pore pressures isochrones are shown, while pore pressures inside the chamber remained lower than outside of it. The instance after the end of an earthquake when the excess pore pressures traces of P3 and P5 of figure 6 intersect with the traces of P4 and P5 was approximately the instance when the solidification front outside of the chamber arrived at the level of its cap. The effect of the top boundary condition is better observed after the second earthquake, since pressures had already started dissipating inside the chambers during the motion. Excess pore pressures matched the top boundary condition early on and stayed at that level while the surrounding soil remained liquefied.

When the solidification front outside of the chamber arrived at the level of the chamber's cap, the total horizontal stress applied to the membrane from the outside soil started reducing, but not as fast as excess pore pressures, since horizontal effective stresses were also gradually restored. The flexible membrane of OA2 would have forced pore pressures inside the chamber to match the outside total horizontal stress at the level of the cap. It is therefore

hypothesised that after solidification outside of the top of the chamber, the traces of P4 and P6 (figure 6) followed the total horizontal stress outside of the chamber's cap. In OA3, hoop stresses in the ring surrounding the cap allowed pore pressures inside the chamber to remain elevated. However, due to the total stress difference, the periphery in OA3 was likely pushed to return towards its initial circular shape, resulting in the additional drop in excess pore pressure observed when the soil surrounding the cap started reconsolidating.

The height of both chambers reduced after the earthquakes. In OA2, the weight of the cap pushed the membrane to expand even further. The rate of displacement recorded by L2 reduced as the soil surrounding the chamber reconsolidated and became more difficult to push into. It is possible that the flexible membrane pushed locally into the surrounding soil while pressures were higher in the chamber than outside, creating small pockets that were locally maintained after reconsolidation. Protrusions along the flexible membrane were visible after the test, when the sand was excavated (figure 11a). In OA3, the recorded reduction of the height of the chamber corresponded to a return towards a more cylindrical shape, driven by the weight of the cap and the increased pressures inside the chamber.

SHEAR STRESS - SHEAR STRAIN RESPONSE

The dynamic shear stress - shear strain response at the level of accelerometers A3 and A4 is presented in figure 12. Stresses and strains were calculated using acceleration data, following the methodology proposed by Elgamal et al. (1996). Special care was given to filtering, as suggested by Brennan et al. (2005).

During the first earthquake, which was of smaller intensity than the second motion, the sand close to the base of the model did not reach liquefaction, allowing the soil at the level of the chambers to experience larger strains (see plots labelled 'b' in figure 12). Indeed, the shear response of the soil was stiffer during the first couple of cycles of the first earthquake, compared to the initial cycles of the second motion, for which excess pore pressures increased more rapidly (see plots labelled 'd' in figure 12).

During the first few cycles of each motion, while excess pore pressure was building up, no significant differences were observed inside and outside of the chambers, except for the second earthquake of OA2. As mentioned before, due to increased shearing a transient drop in excess pore pressures occurred, which was likely facilitated inside the chamber by the proximity of the lower boundary. As the mean effective stress temporarily increased inside the chamber, the soil there became stiffer, justifying the smaller shear strains as compared to the free-field, despite shear stresses being of the same amplitude.

As the earthquakes continued, excess pore pressures increased and the soil softened considerably, as can be seen by comparing plots labelled 'd' and 'e' in figure 12. During the first earthquake, for which shear strains remained high throughout the motion, excess pore pressures inside the chambers remained elevated and the soil maintained a soft shear response, albeit slightly stiffer than at the free-field. This slightly increased shear stiffness inside the chambers was likely due to drainage, enabled by the proximity of the boundaries. Excess pore pressures inside the chambers experienced slightly larger transient drops due to dilation as compared to the free-field, likely due to the proximity of the lower boundary, which limited the level of fluid inflow. The larger transient drops in pore pressure led to the higher shear stiffness observed. Another factor that could have contributed is the periphery of the chambers. The membrane of the chamber in OA2 was flexible (similar to membranes

used in element tests) and is not expected to have introduced significant radial stresses for the levels of deformation observed in these experiments. In OA3, the periphery of the chamber could have locally developed radial stresses when in tension, due to the presence of the fishing line. Radial stress could have promoted a stiffer response inside the chamber. An overall increase in confinement due to the periphery could not have occurred, as the volume inside the chamber was practically constant and its height gradually increased, making it impossible for the whole periphery to have been under tension.

During the second earthquake, shear strains diminished as the sand at the base of the model liquefied. Excess pore pressures inside the chambers dropped as a result of drainage and void redistribution, with effective stresses rising in response (see plots labelled 'c' for EQ2 in figure 12). The same behaviour was not observed in the free-field, where the boundaries were further away and fluid inflow was maintained throughout the motion. The increased effective stresses led to a stiffer shear response, which was more pronounced in OA3.

CONCLUSIONS

Earthquake-induced liquefaction is often regarded as an undrained phenomenon, with undrained element tests forming the basis of our understanding.

In this paper, the effect of drainage was investigated experimentally using two dynamic centrifuge tests. In these tests, drainage out of a part of the soil was restricted, by enclosing it within a chamber. Lateral expansion of the periphery of the chamber was allowed in the first test and restricted in the second.

It was concluded that undrained behaviour was not a realistic assumption for the timescale of an earthquake, in or out of the chamber. Restricting drainage out of the chamber did not produce a response closer to undrained. Instead, by bringing the boundaries closer, drainage became more important, manifesting through localised fluid flow and void redistribution.

The evolution of excess pore pressures was a result of the interplay between drainage and soil skeleton deformation due to shearing. In the free-field, excess pore pressures retained elevated values even with reduced levels of shearing because the boundaries were further away, allowing the level of inflow in an element to be similar to the level of outflow. Fluid flow towards the surface resulted in large co-seismic settlement. This type of response should not be interpreted as undrained.

Inside the chambers, when the level of shear strain imposed by the earthquake was low enough, the effects of drainage became evident through the dissipation of excess pore pressures. The upper boundary of the chamber, under which a fluid film likely formed, defined the level to which excess pore pressures dissipated. The proximity of the lower boundary of the chamber, where fluid flow was zero, allowed larger transient drops in excess pore pressure as the soil entered the dilatancy domain during each half-cycle of loading. A stiffer shear response was produced as a result. Finally, the different periphery of each chamber affected deformations significantly, with one chamber reducing in height during the earthquake and the other increasing. This was a result of the capacity or not for lateral expansion, in combination with the placement of the chamber in the laminar box.

In typical undrained element tests, the boundaries are much closer than in the chambers examined here, significantly reducing the relevant timescale for drainage. Consequently, the

effect of spacial variation of excess pore pressure cannot be captured. However, this effect can be of great importance for the response of liquefied soil in reality, as shown in the centrifuge experiments presented here.

ACKNOWLEDGEMENTS

The centrifuge tests were carried out with the assistance of the technicians of the Schofield Centre, who are hereby acknowledged. The first author would like to thank Qualcomm, the Vergottis family and the Foundation for Education and European Culture for their financial support.

NOMENCLATURE

F	Factor for the relative importance of drainage (Snieder & Van Den Beukel, 2004)
K_f	Bulk modulus of pore fluid
L	Depth of liquefiable layer
T	Timescale for excess pore pressure generation
e	Voids ratio, equal to the volume of voids over the volume of grains of an element
g	Acceleration of gravity
k	Hydraulic conductivity (m/s)
p	Excess pore pressure
t	Time
β	Grain fraction, equal to the volume of grains over the total volume of an element
τ	Shear stress
κ	Permeability (m^2)
μ	Viscosity of pore fluid
ϕ	Porosity, equal to the volume of voids over the total volume of an element
ρ_f	Density of pore fluid
γ	Shear strain
ch	Chamber
ff	Free-Field

REFERENCES

- Adamidis, O., Madabhushi, S. P. G. (2015). *Use of viscous pore fluids in dynamic centrifuge modelling*, International Journal of Physical Modelling in Geotechnics, 15(3), pp.141–149.
- Adamidis, O., Madabhushi, G. S. P. (2016). *Post-liquefaction reconsolidation of sand*, Proceedings of the Royal Society A, 472(2186), pp.20150745.
- Azeiteiro, R. J. N., Coelho, P. A. L. F., Taborda, D. M. G., Grazina, J. C. D. (2017). *Critical State Based Interpretation of the Monotonic Behavior of Hostun Sand*, Journal of Geotechnical and Geoenvironmental Engineering, 143(5), pp.04017004.
- Boulanger, R. W. & Truman, S. P. (1996). *Void redistribution in sand under post-earthquake loading*, Canadian Geotechnical Journal, 33(5), pp.829–834.
- Brennan, A. J., Madabhushi, S. P. G., Houghton, N. E. (2006). *Comparing laminar and equivalent shear beam (ESB) containers for dynamic centrifuge modelling*, Physical Modelling in Geotechnics, 6th ICPMG'06, Taylor & Francis, pp.171–176.
- Brennan, A. J., Thusyanthan, N. I., Madabhushi, S. P. G. (2005). *Evaluation of Shear Modulus and Damping in Dynamic Centrifuge Tests.*, Journal of Geotechnical and Geoenvironmental Engineering, 131(12), pp.1488–1497.
- Doanh, T., Ibraim, E., Mاتيotti, R. (1997). *Undrained instability of very loose Hostun sand in triaxial compression and extension. Part 1: experimental observations.*, Mechanics of Cohesive-Frictional Materials, 2(1), pp.47–70.
- Elgamal, A., Zeghal, M., Taboada, V., Dobry, R. (1996). *Analysis of Site Liquefaction and Lateral Spreading Using Centrifuge Testing Records.*, Soils and Foundations, 36(2), pp.111–121.
- Escribano, D. E., Nash, D. F. T (2015). *Changing anisotropy of G₀ in Hostun sand during drained monotonic and cyclic loading*, Soils and Foundations, 55(5), pp.974–984.
- Goren, L., Aharonov, E., Sparks, D., Toussaint, R. (2010). *Pore pressure evolution in deforming granular material: A general formulation and the infinitely stiff approximation*, Journal of Geophysical Research, 115(B9), pp.B09216.
- Haigh, S. K., Eadington, J., Madabhushi, S. P. G. (2012). *Permeability and stiffness of sands at very low effective stresses*, Géotechnique, 62(1), pp.69–75.
- Ishihara, K. (1993). *Liquefaction and flow failure during earthquakes*, Géotechnique, 43(3), pp.351–451.
- Kamai, R. & Boulanger, R. W. (2012). *Single-element simulations of partial-drainage effects under monotonic and cyclic loading*, Soil Dynamics and Earthquake Engineering, 35, pp.29–40.

Kokusho, T. (2003). *Current state of research on flow failure considering void redistribution in liquefied deposits*, Soil Dynamics and Earthquake Engineering, 23(7), pp.585–603.

Lakeland, D. L., Rechenmacher, A. & Ghanem, R. (2014). *Towards a complete model of soil liquefaction: the importance of fluid flow and grain motion*, Proceedings of the Royal Society A: Mathematical, Physical and Engineering Sciences, 470(2165), pp.20130453-20130453.

Madabhushi, S. P. G. (2014). *Centrifuge Modelling for Civil Engineers*, Taylor & Francis, London.

Madabhushi, S. P. G., Houghton, N. E., Haigh, S. K. (2006). *A new automatic sand pourer for model preparation at University of Cambridge*, Physical Modelling in Geotechnics, 6th ICPMG'06, Taylor & Francis, pp.217–222.

Madabhushi, S. P. G., Schofield, A. N., Lesley, S. (1998). *A new Stored Angular Momentum (SAM) based earthquake actuator*, Proc. of The Intern. Conf. Centrifuge '98, Balkema, pp.111–116.

Mitrani, H. (2006). *Liquefaction Remediation Techniques for Existing Buildings*, PhD Thesis, University of Cambridge.

Miyamoto, J., Sassa, S., Sekiguchi, H. (2004). *Progressive solidification of a liquefied sand layer during continued wave loading*, Géotechnique, 54(10), pp.617–629.

Sento, N., Kazama, M., Uzuoka, R., Ohmura, H., Ishimaru, M. (2004). *Possibility of Postliquefaction Flow Failure due to Seepage*, Journal of Geotechnical and Geoenvironmental Engineering, 130(7), pp.707–716.

Snieder, R., Van Den Beukel, A. (2004). *The liquefaction cycle and the role of drainage in liquefaction*, Granular Matter, 6(1), pp.1–9.

Stringer, M. E. & Madabhushi, S. P. G. (2009). *Novel Computer-Controlled Saturation of Dynamic Centrifuge Models Using High Viscosity Fluids*, Geotechnical Testing Journal, 32(6), pp.102435.

Vaid, Y. P. & Eliadorani, A. (1998). *Instability and liquefaction of granular soils under undrained and partially drained states*, Canadian Geotechnical Journal, 35(6), pp.1053-1062.

Vaid, Y. P. & Eliadorani, A. (2000). *Undrained and drained (?) stress-strain response*, Canadian Geotechnical Journal, 37(5), pp.1126-1130.

Wang, H. F. (2000). *Theory of Linear Poroelasticity With Applications to Geomechanics and Hydrogeology*, Princeton University Press, Princeton, N.J.

Table 1. Properties of Hostun sand (after Mitrani (2006) and Haigh et al. (2012)).

e_{max}	e_{min}	G_s	ϕ_{crit}	$k \text{ (mm/s)}$
1.010	0.555	2.65	33°	1

Table 2. Factor of significance of drainage F , according to Snieder & Van Den Beukel (2004).

	Free-field		Chamber	
	$EQ1$	$EQ2$	$EQ1$	$EQ2$
F	6.0	2.2	39.8	14.9

Figure 1. Cross-section of the model in centrifuge experiments OA2 and OA3. A laminar box was used. Transducer L3 was in place only for test OA3. Dimensions in model scale.

Figure 2. Sketches of the chambers, as used for each test. Dimensions in model scale.

Figure 3. Preparation of the chambers: a. The disks, along with the fittings and the top LVDT rod. b. The latex sheet with sand stuck to its inner side. c. The chamber of test OA2, without the top cap, temporarily supported inside a PET cylinder. d. The chamber of test OA3. The fishing line, the layer of liquid rubber, the ring and the aquarium silicone connection are visible. e. Inside the chamber. f. Outside of the chamber.

Figure 4. Sketch of the chamber, the pipes, and the valves layout.

Figure 5. Time histories of excess pore pressures for the ‘free-field’ soil column (figure 1). The presence of the chamber in the right half of the laminar box did not affect the excess pore pressure generation and dissipation at the left half.

Figure 6. Time histories of excess pore pressures, chamber (ch) displacement and free-field settlement (ff), and input acceleration. For test OA2, chamber displacement corresponds to the trace of L2 (figure 1), whereas for test OA3 it corresponds to the change of the height of the chamber. All traces are in model scale.

Figure 7. Excess pore pressure isochrones inside the chamber, while excess pore pressures remained lower than at the free-field. The dots correspond to the values recorded by P4 and P6. Excess pore pressures reduced, even during the earthquake, to match the excess pressure of a fluid film which likely formed just below the cap of the chamber. In model scale.

Figure 8. Assumption for the deformation experienced by the chamber for typical half-cycles of each test. a. Test OA2, box moving to the left. b. Test OA2, box moving to the right. c. Test OA3, box moving to the left. d. Test OA3, box moving to the right.

Figure 9. Rocking of the soil mass occurred within the box. When L1 recorded a peak, L2, at the other end of the box, recorded a valley, signifying rocking of the soil mass. The oscillations of L1 and L2 follow the cycles of the input acceleration, as recorded by A9. The traces are in model scale.

Figure 10. Upwards movement of the cap of the chamber corresponded to a drop in excess pore pressure. Traces in model scale.

Figure 11. Photos of the chamber after the excavation of the model. Ridges were observed around the expandable chamber of test OA2. Some residual rotation was observed for the cap of the chamber, with the side closer to edge of the box being higher than the one closer to the centre.

Figure 12. Shear stress - shear strain plots. The line for the free-field corresponds to accelerometer A3 and the line for the chamber corresponds to accelerometer A4. a. Dynamic shear stress time history. b. Shear strain time history. c. Dynamic shear stress versus vertical effective stress. The circular marker corresponds to the start of the earthquake and the square to the end. d. Stress-strain loops during the first cycles of loading, corresponding to the first grey area of plots a and b. e. Stress-strain loops later in the earthquake, corresponding to the second grey area of plots a and b.

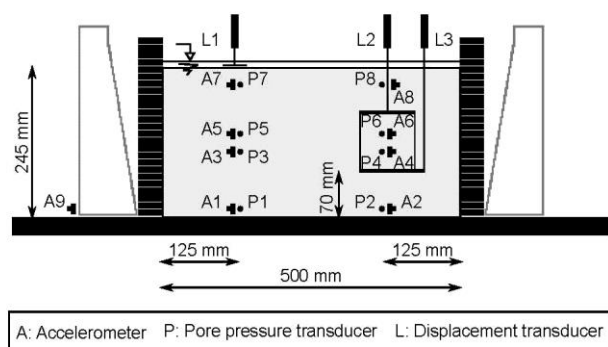


Figure1.jpg



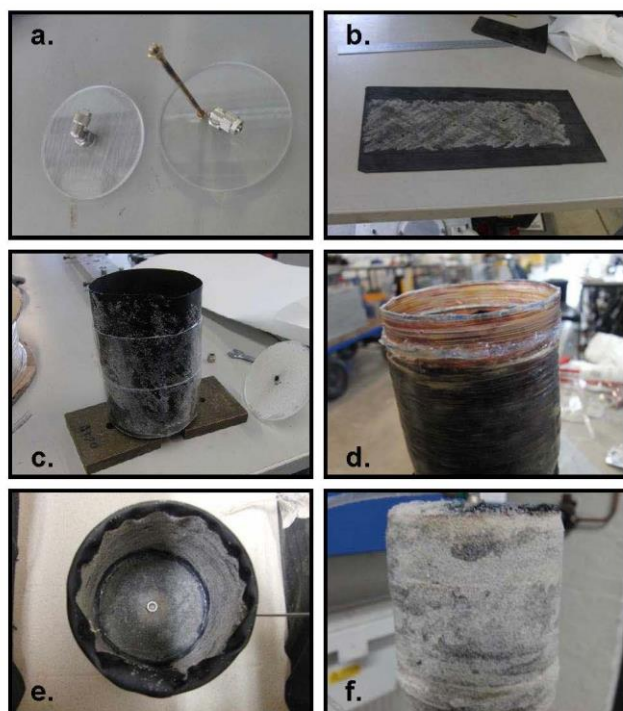


Figure3_Colour.jpg

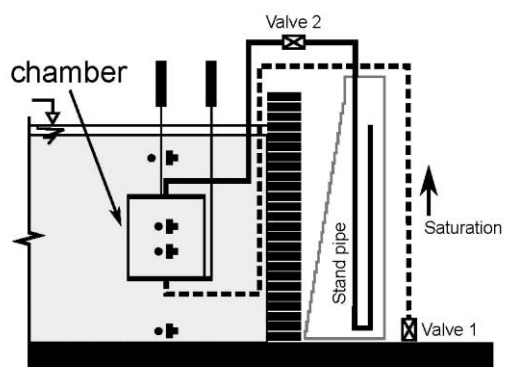


Figure4.jpg

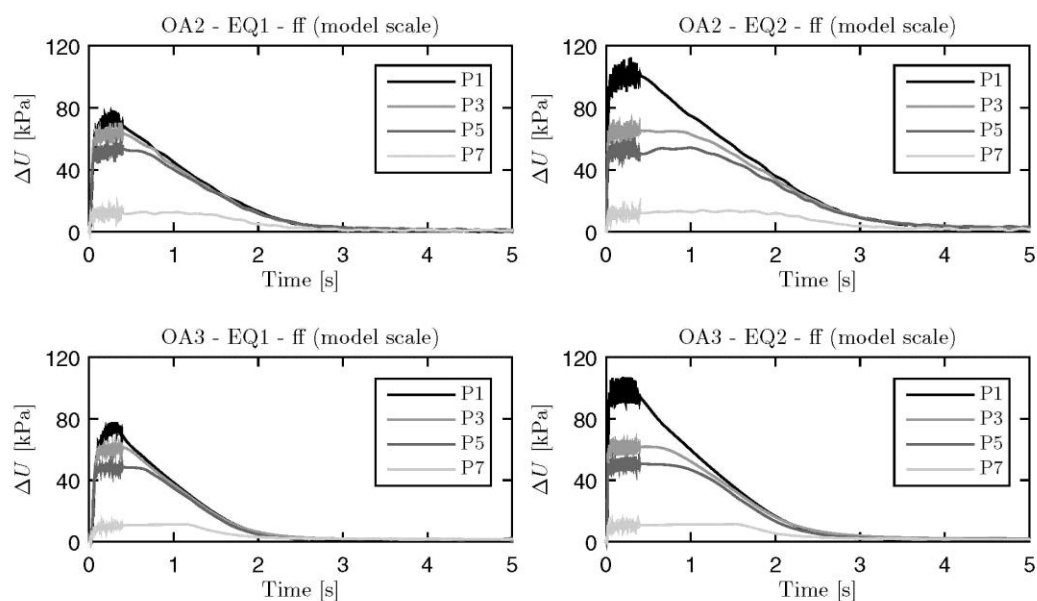


Figure5_Modelscale_BW.jpg

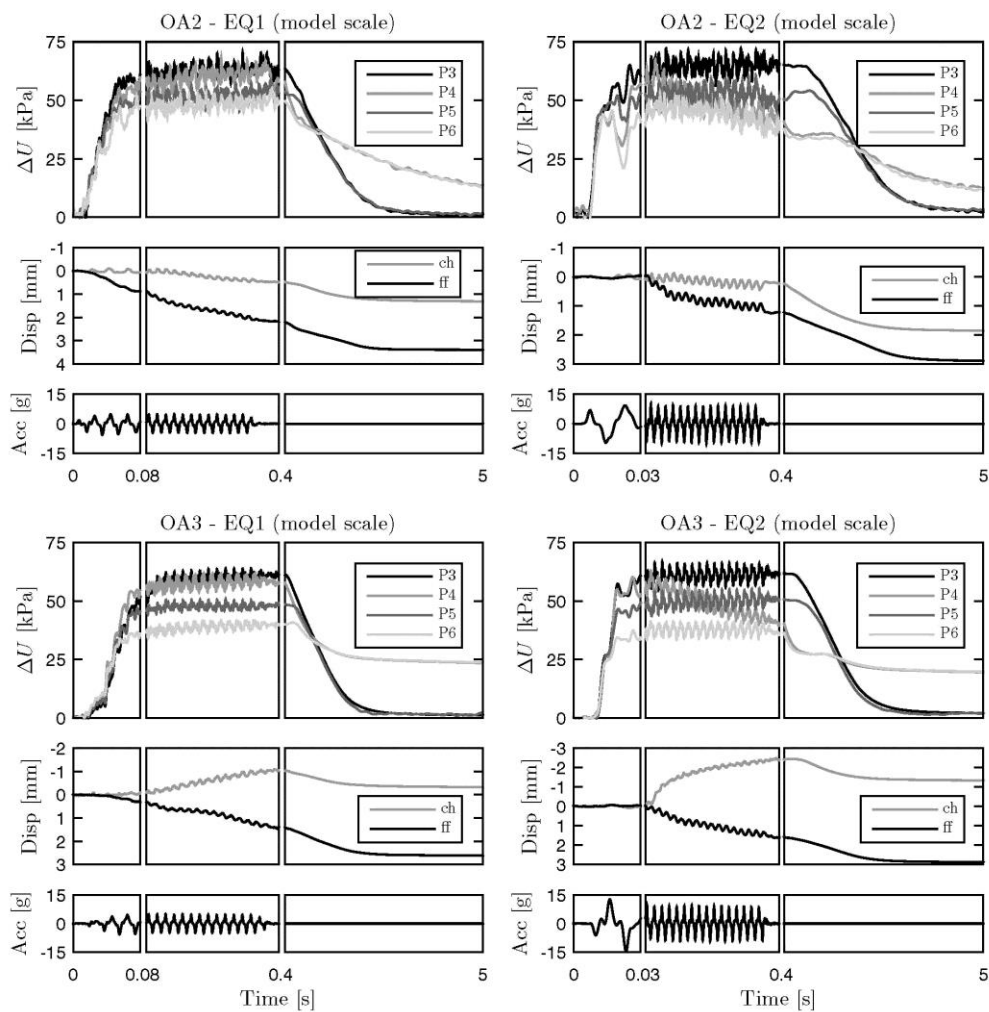


Figure6_Modelscale_BW.jpg

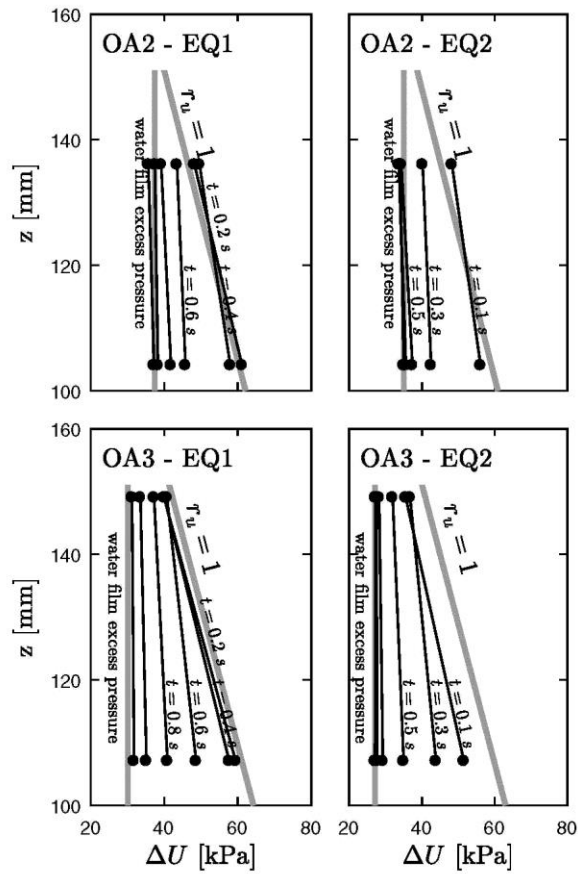


Figure7.jpg

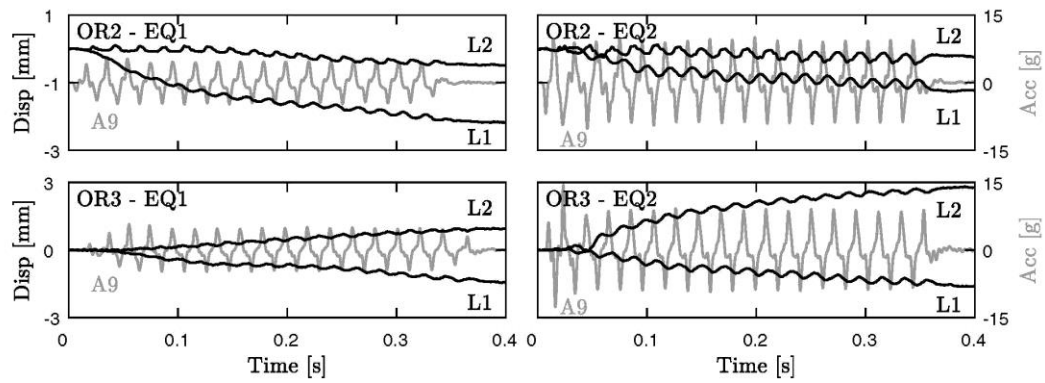


Figure8_BW.jpg

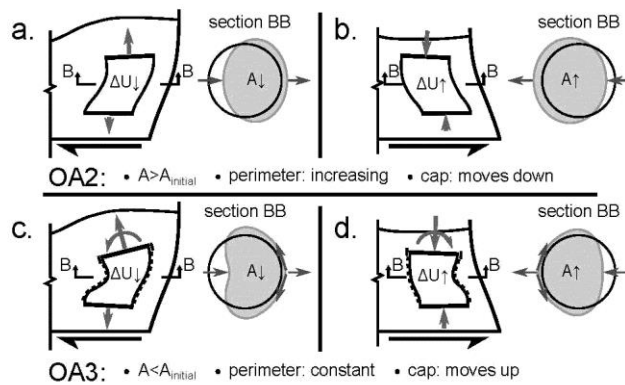


Figure9.jpg

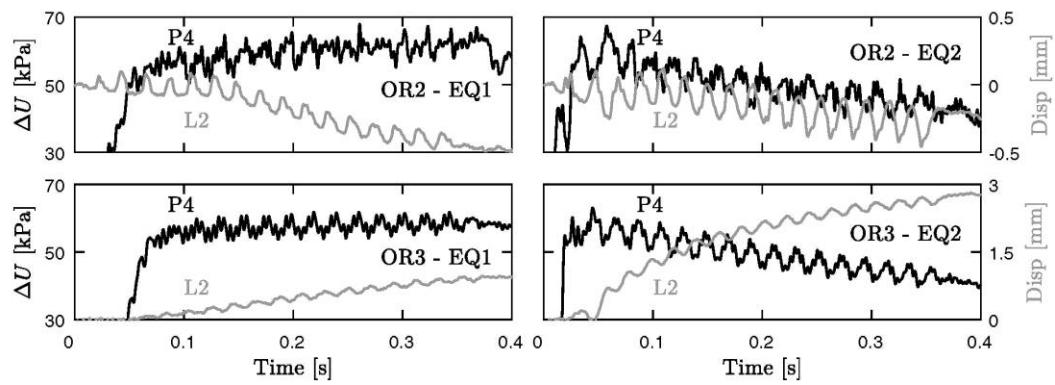


Figure10_BW.jpg

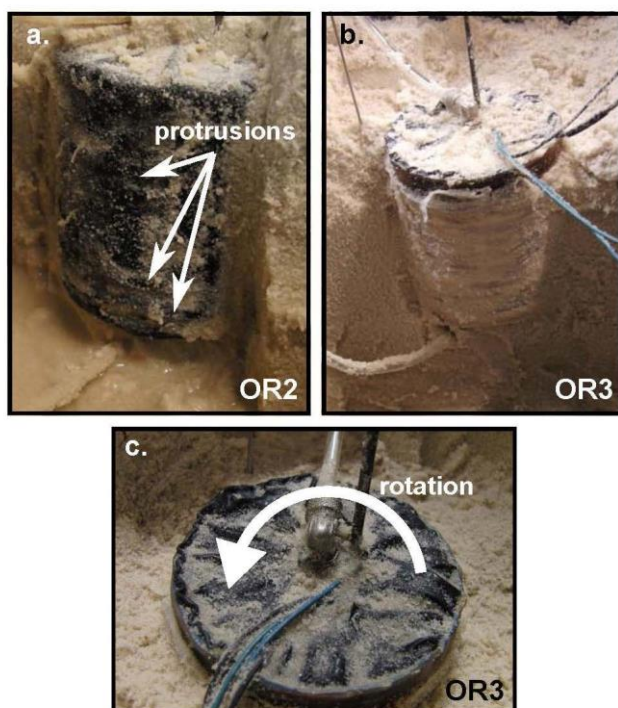


Figure11_Colour.jpg

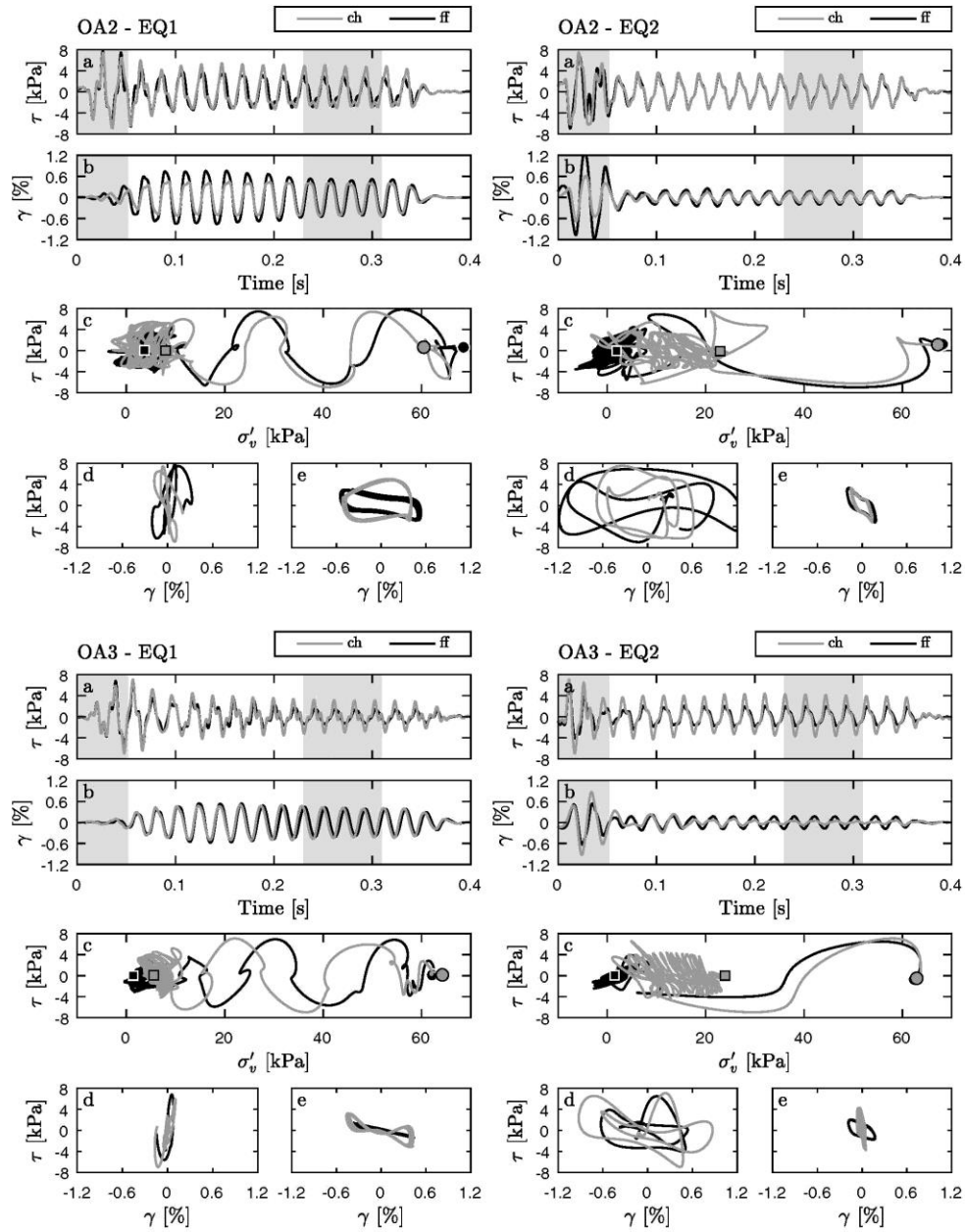


Figure12_BW.jpg